# Perspectives on electrical neural recording: a revisit to the fundamental concepts

**Liang Guo**[1,2]

[1] Department of Electrical and Computer Engineering, The Ohio State University, Columbus, OH, United States of America
[2] Department of Neuroscience, The Ohio State University, Columbus, OH, United States of America

E-mail: guo.725@osu.edu

Received xxxxxx
Accepted for publication xxxxxx
Published xxxxxx

## Abstract

*Objective.* This paper aims to promote understanding on the fundamental concepts and mechanisms of extracellular electrical neural recording. *Approach.* First, the electrode-electrolyte interface is reviewed to clarify some of the frequent misunderstandings. Second, analytical solutions to the extracellular field potential and recorded signal are derived based on equivalent electrical circuit models, using a planar substrate microelectrode as a particular example. And third, factors affecting the recording quality are thoroughly assessed. *Main results.* Passive neural recording electrodes function as a pure capacitor. The extracellular field potential has two phases, with its subthreshold depolarization phase proportional to the first time derivative of the membrane depolarization and its action potential phase proportional to the negative first time derivative of the intracellular action potential. The recorded signal represents a portion of the extracellular field potential with both amplitude attenuation and phase distortion according to a voltage-divider circuit formed between the recording electrode and amplifier. A larger cell, a larger cell-substrate junctional membrane area, and a tighter membrane-substrate seal all help to improve the recording quality, while the effective electrode impedance should be minimized and the effective amplifier's input impedance maximized. *Significance.* This paper develops in-depth insights to offer a clear image on the recording mechanism, nature of the signal, and interplays between key interface parameters. This work will make a foundational contribution to the field by providing such an in-depth understanding on this topic to clear the widespread ambiguities and confusions and inform rational neural electrode designs and proper interpretations of neural recordings.

Keywords: extracellular action potential, equivalent electrical circuit model, electrode-electrolyte interface, electrode impedance, microelectrode array, neural recording, recording mechanism, signal-to-noise ratio.

## 1. Introduction

Electrical neural recording has played a key role in modern neurophysiology and neural prosthetics. While intracellular recording, such as using glass micropipette or patch clamp electrodes, is valuable to neurophysiological studies with the acquisition of a signature waveform of the action potential (AP), extracellular recording, though complicated by the location, size, shape of the electrode, as well as neighboring neural structures [1], is more practical for prolonged recording applications in both fundamental neuroscience investigations and neural prosthetics. More importantly, it is the recording modality for most neural interfaces.

 

However, for many people in the neural interfaces field and others who use electrical neural recordings very often, the recording mechanism is of great ambiguity and confusion. Although the literature provides some basis on this topic [2-8], the dispersive and piecewise nature of knowledges on this topic makes it hard for the majority to develop an accurate and comprehensive understanding on it. This knowledge gap unfortunately has led to flawed neural electrode designs and characterizations, poor interpretations of the distorted recordings, and inconsistencies in findings among papers published from different research groups. It is thus imperative to address this gap to mitigate confusions and promote understandings on the fundamental concepts and mechanisms. As such, this paper intends to revisit the fundamentals for electrical neural recording with a focus on extracellular recording and clarify some of the frequent misunderstandings in literature.

## 2. The electrode-electrolyte interface

The mechanism of recording biopotentials may seem straightforward at first sight to many people who work with electronic circuits: two electrodes each connecting to one input terminal of a differential amplifier are placed on or in the biological tissue with a certain distance so that the potentials at each electrode site are distinct; the electrodes when in contact with the tissue instantaneously achieve isopotential with the local tissue; because it is assumed that no current flows into either terminal of the differential amplifier, the potential difference of the tissue at the two electrode sites is picked up by the input terminals of the amplifier.

However, the real mechanism is far more complicated than this layman interpretation. This is because any biopotential recording involves physiological fluids, *i.e.*, electrolytic solution, at the immediate electrode surface, making the electrical signal transduction from ion-based in the tissue to electron-based in the solid-state electrode a complicated process governed by thermodynamics and electrochemistry. Thus, it is essential to first develop an in-depth understanding of the electrode-electrolyte interface.

### *2.1 The electrode-electrolyte phase boundary*

A phase transition boundary is developed when a solid (conductor, semiconductor, or insulator) is brought in contact with a salt (electrolytic) solution. During the initial transition process, atoms in the solid surface may lose electrons to the solution and become dissolved, or ions in the electrolyte may gain electrons from the solid and become deposited/adsorbed on its surface. Over a short period of time when this solid-electrolyte interface achieves a thermodynamic equilibrium, on the one hand, a thin charge (electron or hole) layer forms immediately underneath the solid surface; and on the other hand, complementary ionic charges spatially coalesce in the electrolytic solution to yield a concentration gradient and a charge gradient (together called an electrochemical gradient) conventionally described by the so-called *electrical double layer* (EDL). As a result, an electrostatic field is formed starting from the immediate solid surface and extending into the electrolytic solution, and a characteristic electrode potential (*i.e.* the *surface potential* $E_0$) is established, which is associated with the solid's material type. The Bockris/Devanathan/Müller (BDM) model describes this EDL as a cascade of three regions (Figure 1) [6, 8-12]: (1) an *inner Helmholtz plane* (IHP) formed by a layer of adsorbed water molecules with highly oriented dipole moments on the solid's surface, (2) an intermediate *outer Helmholtz plane* (OHP) formed by solvated (hydrated, in aqueous solutions) ions, and (3) a *Gouy-Chapman diffuse layer* beyond the OHP with an ionic charge density decaying outward due to increasing thermal motions of ionic species in the solution. The IHP and OHP together are summarized as the *Stern layer*. Additionally, some specifically adsorbed and partially solvated ions can also appear in the IHP, as proposed by D. C. Grahame.

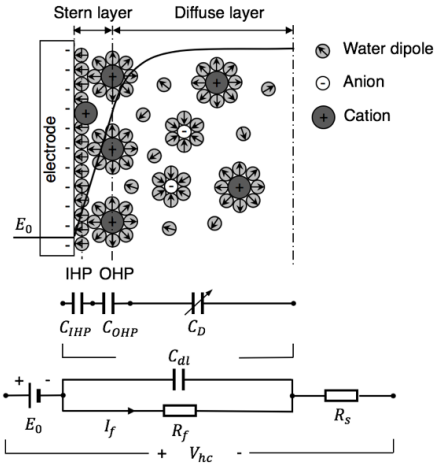


**Figure 1.** Electrode-electrolyte interface at equilibrium and its equivalent electrical circuit model. The EDL comprises the Stern layer (including the IHP and OHP) and the diffuse layer. In the Stern layer, the magnitude of electric potential decreases linearly with distance, while in the diffuse layer, it decreases exponentially. A series of three capacitors models the IHP, OHP, and diffuse layer, respectively, which is usually lumped together as $C_{dl}$ in the overall equivalent circuit model. $E_0$: surface potential of the electrode, $R_f$: faradaic resistance through redox reactions, $I_f$: faradaic current, $R_s$: spreading (or series) resistance of the bulk electrolyte, and $V_{hc}$: half-cell potential.

The electrostatic field in the EDL has two regions: In the Stern layer, the magnitude of potential decreases linearly with distance from the solid's surface, and the boundary potential at the outer edge of the OHP is referred as the *Stern potential*. In the diffuse layer, the magnitude of potential decreases exponentially. The thickness of this diffuse layer is called the *Debye length* [8]. In aqueous solutions, it is typically on the scale of a few nanometers and decreases with increasing ion concentration.

The electrical properties of this EDL is conventionally modeled as a series of three capacitors, representing the spatial

ionic charge distributions in the IHP, OHP, and diffuse layer, respectively [6]. The full equivalent electrical circuit model also includes a parallel faradaic resistance $R_f$, the surface potential $E_0$ of the electrode and the series resistance $R_s$ of the bulk electrolyte, as depicted in Figure 1. The $R_f$ further consists of two components (not depicted): the crossover electron transfer that is proportional to the exchange current density and the mass transport phenomena that are modeled with the so-called *Warburg impedance* (also called the *constant phase element*) [8]. In the physiological frequency range, the bulk electrolytic solution is considered as a pure resistor $R_s$ [8, 13]. For example, phosphate buffered saline (PBS) has a resistivity of ~0.09 Ω·m at room temperature [13], which give $R_s$ a value of around 1 kΩ for an electrode immersed in the center of a 10 cm diameter Petri dish.

### *2.2 The electrochemical cell*

Knowledge on electrode systems used in neural recording and stimulation has been derived from the general electrochemistry. The configuration of a pair of electrodes on or in a wet biological tissue essentially forms an electrochemical cell. There are two basic types of electrochemical cells: *galvanic* and *electrolytic* (Figure 2). In both types, the EDL plays a vital role in conversion between electronic and ionic currents through redox reactions. Galvanic cells generate an electrical current from spontaneous redox reactions taking place within the cell, due to a difference between the surface potentials of the two electrodes (made of different materials), *e.g.* a discharging battery. Electrolytic cells use an electrical current to cause non-spontaneous redox reactions, for example in electrodeposition/electroplating.

In a galvanic cell, chemical energy in the electrolytic solution is converted to external electrical energy through redox reactions, which take place on the electrodes' surfaces. To make the galvanic cell, the two electrodes need to have different surface potentials and thus be made of two different materials. Once connected to a resistive load via leads, the electrode having a higher surface potential will draw electrons via the lead from the electrode with a lower surface potential, and an equilibrium will be achieved between the two electrodes at a common potential, only if these deviations from their surface potentials do not exceed the thermodynamic thresholds for redox reactions to take place on the electrodes' surfaces, which attempt to restore the respective surface potentials. However, if these thresholds are exceeded, the ongoing complementary redox reactions at the electrodes will circulate electrons in the electronic half-circuit, while closing the circuit in the electrolytic solution by migrations of reactant ions toward the electrode surfaces to sustain the redox reactions. As a result, a dynamic equilibrium will be achieved with an electrode potential somewhere in-between the targeting common potential, and the surface potential of each electrode is sustained, while the complementary redox reactions are taking place. In this situation, the anode is the electrode to which reactant anions *actively migrate* for oxidation; therefore, the accumulation of these anions makes the anode negative in polarity (Figure 2). Similarly, the cathode is the electrode to which reactant cations actively migrate for reduction; and the accumulation of these cations makes the cathode positive. It is reasonable to assume that the electrode having a higher surface potential will become the cathode, while the one with a lower surface potential becomes the anode.

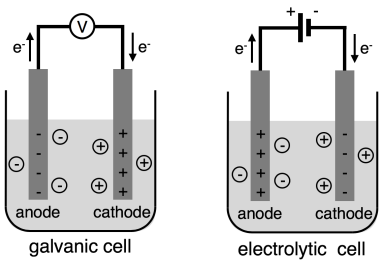


**Figure 2.** Two basic types of electrochemical cells.

In contrast, in an electrolytic cell, externally supplied electrical energy is converted to chemical energy in the electrolytic solution through redox reactions happening on the electrodes' surfaces. To make the electrolytic cell, the two electrodes don't have to be made of two different types of materials, rather are frequently of the same material. The electrode connecting to the negative terminal of the voltage source becomes negative in polarity and attracts cations in the electrolytic solution (Figure 2). As electrons are provided at this electrode, if the potential exceeds the threshold of a reduction reaction in the solution, it will take place, making this electrode the cathode. Similarly, the electrode connecting to the positive terminal of the voltage source becomes positive and attracts anions in the solution. If the electrode potential exceeds the threshold of an oxidation reaction in the solution, it will take place, making this electrode the anode. It should be noted that the reduction or oxidization half-reaction cannot happen alone. A complementary reaction pair is always tied together. The circuit is closed in the solution through *passive migration* (being electrostatically attracted) of the reactant ions toward the respective electrodes and ionic-to-electronic transduction at the electrodes via the complementary redox reactions.

### *2.3 The half-cell potential*

The concept of *half-cell potential* $V_{hc}$ is conventionally used to describe the potential of an electrode with reference to the far-away bulk electrolyte. It is defined in the context of a galvanic cell where a matching pair of redox half-reactions occurs on the surfaces of an electrode pair, as the configuration with one electrode represents half of the cell. Its value depends on temperature, pressure and electrolyte concentration. This concept can also be extended to the

electrolytic cell (*e.g.*, neural stimulation electrode systems) and the non-redox cell (e.g., neural recording electrode systems). The two half-cell potentials add up to form the overall cell potential, which can be measured directly. However, neither of the half-cell potentials can be measured in isolation, as an electrochemical cell requires a pair of electrodes. Thus, an electrode's half-cell potential is usually measured with reference to a standard hydrogen electrode (SHE) with which it forms a galvanic cell. As the potential of the SHE is defined as 0 V by convention, the measurement will read out the electrode's half-cell potential directly. If this measurement is taken at the standard state (*i.e.*, 1 M, 1 atm, 25 °C, and pH = 7), the measured value is more commonly known as the *standard electrode potential*, which is a property of the electrode material itself. Since the oxidation potential of a reversible half-reaction in a redox reaction is the negative of its reduction potential, the oxidation half-reaction occurring on an electrode is conventionally converted to a reduction reaction, thus the associated half-cell potential is commonly written as the *standard reduction potential*. With this measurement configuration in mind, the half-cell potential can be viewed as the potential difference between an electrode's surface and the far-away bulk electrolyte where the 0 V SHE is placed, thus, $V_{hc} = E_0 + I_f R_f + V_{R_s}$ (where $V_{R_s}$ is the voltage across $R_s$ in Figure 1). However, in practical situations where two regular electrodes are used and placed not very far apart, $V_{hc} = E_0 + I_f R_f + \frac{V_{R_s}}{2}$.

For both biocompatibility reason and electric field recording purpose (where the $I_f$ will be a contaminating electrochemical noise), no redox reaction should occur on passive neural recording electrodes (*i.e.*, $R_f = \infty$ and $I_f = 0$) [2], which thus are frequently made of noble metals (*e.g.*, Pt and Au) that are inert in physiological solutions. Furthermore, the pair of electrodes are often made of the same material, *i.e.* no surface potential difference between them, and during recording they each are connected to an input terminal of a differential amplifier, which has a very high input impedance, rather than to each other directly via a load. Thus, the neural recording electrode system is a *non-redox* cell in a broad sense, so is the stimulation electrode system in the absence of stimulation current. But, a surface potential is assumed still to build up on the electrode's surface through capacitive mechanism once the EDL achieves equilibrium. Additionally, because no current flows through $R_s$ at equilibrium, the equivalent circuit of EDL in Figure 1 is reduced to purely capacitive with $V_{hc} = E_0$. Unfortunately, knowledge on such a surface potential for neural electrodes working in physiological solutions is absent in the literature, and the concept of half-cell potential is frequently misused on neural electrodes.

The presence of this surface potential $E_0$ with a magnitude in the several hundred millivolts scale on the electrode thus requires a means in the differential amplifier to block this large DC bias in order to prevent the amplifier from saturation. The *common-mode rejection* is exactly for this purpose. Differential amplifiers usually have an excellent common-mode rejection ratio (CMRR) which can effectively cancel out this common DC bias present on both of the recording electrode pair. It thus implies that the recording electrode pair needs to be made of the same material and of the same size in order to have the same surface potential for an effective cancellation. Because the Debye length of EDL in aqueous solutions is only a few nanometers and the distance between a cell membrane and a substrate is no smaller than 40 nm due to repulsive interactions between membrane adhesion and substrate-coated extracellular matrix (ECM) proteins [14], existence of such a DC potential on the electrode surface won't disturb activities of adjacent cells, however, the charged surface can affect cell adhesion to it through interaction with membrane adhesion and ECM proteins.

### *2.4 Electrode polarization*

The phenomenon of *electrode polarization* concerns the process when charges pass across the EDL to initiate faradaic (redox) reactions in an electrochemical cell. It essentially regards to the extra voltage developed in the electrolyte of the EDL due to resistive faradaic reaction products. This resistive conducting path is commonly modeled as the faradaic resistance $R_f$ (Figure 1). The faradaic current $I_f$ flowing through this $R_f$ contributes an additional serial component to the half-cell potential across the EDL, so that $V_{hc} = E_0 + I_f R_f + V_{R_s}$. This additional potential drop is defined as the *overpotential* $\eta = I_f R_f$. The electrode therefore is operating at a new dynamic equilibrium where active faradaic reactions are taking place.

There are two extreme types of electrodes: *perfectly polarizable electrodes* cannot pass charges cross the EDL when a current passes, *i.e.* no faradaic reaction occurs ($I_f = 0$). The current merely results from transient capacitive charge redistributions across the EDL, which is thus purely capacitive with $R_f = \infty$ and $\eta = 0$ (Figure 1). As such, this type of electrodes are perfectly capacitive in nature and cannot pass through DC currents. These electrodes are perfect to serve as neural recording electrodes. For example, polished Au or Pt electrodes are considered to be nearly perfectly polarizable at small currents and commonly used as neural recording electrodes.

In contrast, *perfectly non-polarizable electrodes* pass charges unhinderedly across the EDL with no polarization developing in the electrolyte. The EDL behaves like a short wire with $R_f = 0$ and $\eta = 0$ (Figure 1). This behavior is caused by the ultra-fast kinetics of the faradaic reactions. These electrodes are perfect to serve as reference electrodes, as their potential do not change from the equilibrium potential when current passes. For example, the Ag/AgCl reference electrode are considered non-polarizable. For those reversible

non-polarizable electrodes onto which the redox products remain adsorbed, they are perfect as neural stimulation electrodes, because (1) electrical currents can be passed without corroding the electrode and changing the chemical environment in the vicinity of the electrode (*e.g.*, the overpotential, if beyond the water electrolysis window (-0.6–0.8 V for Pt electrode), can cause water electrolysis) and (2) no overpotential develops in the EDL to risk in tissue injury and consume excess power. Pt and $IrO_2$ electrodes are such examples.

Most real electrodes have characteristics in-between these two extremities. The DC performance of their EDL behaves as a faradaic resistor with a finite value (Figure 1). Up to a certain voltage or current density range across the EDL, the polarization can be described with a linear *V-I* relationship whose slope is designated as $R_f$. Beyond this range, the excess overpotential can severely distort the $I_f$ path in the EDL. Meanwhile, the double-layer capacitance $C_{dl}$ will increase with increasing voltage due to decrease of the EDL thickness by the increasing electric field strength.

It is noted that within the physiological voltage range, the process of passive neural recording only involves purely capacitive charge transductions across the EDL in the absence of any faradaic reactions [2]. The current through the EDL exclusively goes through the $C_{dl}$. Thus, the $R_f$ path in the equivalent circuit is open and no overpotential will be built in the EDL, in contrast to neural stimulation on which excellent reviews exist, *e.g.* ref. [15].

## 3. The mechanism of electrical recording

Besides understanding the EDL at the electrode-electrolyte interface, the mechanism of neural recording cannot be revealed without elucidating the full equivalent electrical circuit of the electrode recording system.

### *3.1 The intracellular action potential (iAP)*

During the initiation and development of AP, there are three primary active ionic currents involved sequentially (Figure 3): an inward $I_{Stim}(j\omega)$ either injected externally or coming from synaptic inputs for subthreshold depolarization, an inward $I_{Na}(j\omega)$ for superthreshold depolarization, and an outward $I_K(j\omega)$ for repolarization. We can define an overall AP current as $I_{AP}(j\omega) = I_{Na}(j\omega) - I_K(j\omega)$. Both $I_{Stim}(j\omega)$ and $I_{AP}(j\omega)$ act to positively charge the inner side of the overall membrane capacitor $C_m$ to produce the sequential AC transmembrane voltages $V_{msub}(j\omega)$ and $V_{mAP}(j\omega)$, so that

$$I_{Stim}(j\omega) = C_m \cdot j\omega V_{msub}(j\omega) \quad (1)$$

$$I_{AP}(j\omega) = C_m \cdot j\omega V_{mAP}(j\omega) \quad (2)$$

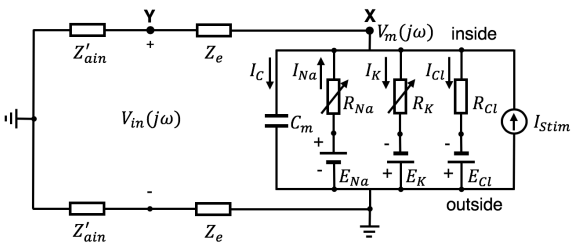


**Figure 3.** Equivalent electrical circuit of excitable cell membrane and setup of intracellular recording.

During subthreshold depolarization, the leaking current through the passive membrane resistance $R_m$ is ignored, as $R_m$ is very high, *e.g.* 150 ~ 600 MΩ for HEK293 cells [2], and the membrane time constant $\tau_m = R_m C_m$, which characterizes the rate the leaking current through $R_m$ discharges $C_m$, is more than one order of magnitude larger than the durations of the subthreshold depolarization and the AP [2, 16]. An alternative justification is that given values of the membrane resistance and capacitance, the majority of passive membrane current flows through $C_m$ at 1 kHz in the parallel circuit, according to $\left|\frac{I_{C_m}}{I_{R_m}}\right| = \omega R_m C_m = \omega\tau$.

During the AP, the following *virtual capacitive current* concept holds [17]. For an imaginary neuron suspended in an electrolyte and referring to Figure 3, during the AP, there is a membrane capacitive current $I_C(j\omega) \approx -I_{AP}(j\omega)$ to close the circuit. As the neuron has uniform current densities (current per unit membrane area) across its entire membrane surface, the capacitive current balances the inward $Na^+$ current during the depolarization phase and the outward $K^+$ current during repolarization. A close scrutinization of this capacitive current from the biophysics aspect of membrane depolarization and repolarization makes us aware that it is different in nature from the capacitive current $I_{C0}(j\omega) \approx I_{Stim}(j\omega)$ during the subthreshold depolarization, which crosses the membrane and flows into the extracellular space. In contrast, $I_C(j\omega)$ does not flow into the extracellular space. Its existence is merely a passive consequence of the discharging or recharging of the transmembrane voltage $V_{mAP}(j\omega)$ by the $I_{Na}(j\omega)$ or $I_K(j\omega)$ according to $I_C(j\omega) = C_m \cdot j\omega V_{mAP}(j\omega)$. Take the discharging phase by $I_{Na}(j\omega)$ as an example. At rest, the membrane is negatively charged inside with anions accumulated on the inner membrane surface and cations on the outer membrane surface. When the subthreshold depolarization reaches the AP threshold, noticeable $Na^+$ ions start to flow across the membrane from the outside. The transportation of one $Na^+$ ion from the outside to the inside, where it "cancels out" an anion, depolarizes (reduces) the $V_{mAP}(j\omega)$, which requires removal of one charge from both sides (a positive charge from the outside and a negative charge from the inside) of the membrane capacitor $C_m$ according to $Q = C_m V_{mAP}(j\omega)$. Interestingly, this process automatically meets this requirement of charge pair removal without an actual current flowing to either the extracellular or intracellular space. This conclusion can be similarly extended to the recharging phase where the $K^+$ current takes effect. Thus, this type of transmembrane capacitive current $I_C(j\omega)$ is termed as a "virtual" current.

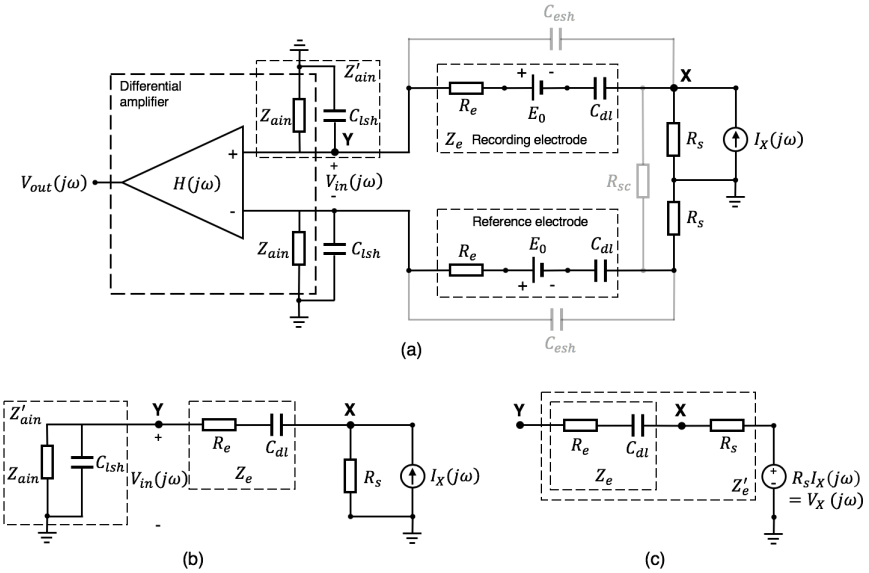


**Figure 4.** The equivalent electrical circuit formed between the recording electrode and amplifier input. The extracellular AP propagating to the edge (Point X) of EDL of the recording electrode is represented as a current source $I_X(j\omega)$. The recording and reference electrodes are assumed to be made of the same materials and geometric dimensions, thus having the same electrical properties. (a) The full equivalent circuit. (b) The reorganized voltage-divider circuit in the context of AC signal transmission. (c) The current source can be converted to an equivalent voltage source using *Thevenin's Theorem*, where $R_s$ appears as the internal resistance of both signal source. $R_s$: spreading resistance, $R_{sc}$: potential resistive coupling through the electrolytic solution between the recording and reference electrodes (if the two are placed far away so that $R_{sc} = \infty$, this resistive coupling can be ignored), $C_{dl}$: EDL capacitance, $E_0$: electrode surface potential (in AC circuit, this electromotive force is equivalent to a short wire), $R_e$: resistance of the electrode material, $C_{esh}$: shunt capacitance across the insulation between the electrode shaft and surrounding electrolyte (if the electrode is properly designed and fabricated, it can be ignored), $Z_e$: the effective electrode recording impedance, $C_{lsh}$: cumulative shunt capacitance along the lead and connector between the electrode and amplifier input terminal, $Z_{ain}$: input impedance of the amplifier, $Z'_{ain}$: the effective input impedance of the amplifier, $V_{in}(j\omega)$: voltage appearing at the input terminals of the differential amplifier, $V_X(j\omega)$: the potential at Point X in the absence of the recording electrode, $Z'_e$: the conventional electrode impedance measured in an open-field physiologically relevant electrolyte using EIS. The *GND* electrode is placed far away.

Taken together, these justifications make the above assumptions of $I_{C0}(j\omega) \approx I_{Stim}(j\omega)$ and $I_{AP}(j\omega) = I_{Na}(j\omega) - I_K(j\omega)$ reasonable approximations.

### *3.2 Mechanism of electrical recording in an electrolyte*

In the electrolyte, the flow of an ionic current establishes an electric field that can exert a force on electric charges in this conductor. This force is what we measure in the form of a potential difference [18]. In Figure 4, with the signal ground *GND* placed far away and in the absence of the electrode, the electrical potential at an imaginary Point X in the electrolyte is determined by Ohm's law through $V_X(j\omega) = R_s I_X(j\omega)$, where $I_X(j\omega)$ is the diverging ionic current from Point X and $R_s$ is the resistive path from Point X to *GND* through which $I_X(j\omega)$ dissipates to the *GND*. Therefore, for a given $I_X(j\omega)$, the field potential $V_X(j\omega)$ at that point depends on the effective impedance of the leaking paths for $I_X(j\omega)$ [19]. This perspective is supported by, for example, the finding that the lumen of a microchannel can effectively boost the amplitude of extracellularly recorded APs [20, 21], because of the substantial increase of $R_s$ in the microchannel. It is worth noting that, by applying the Thevenin's Theorem, the current source $I_X(j\omega)$ in Figure 4b can be converted to an equivalent voltage source $V_X(j\omega) = R_s I_X(j\omega)$ with the same internal source resistance $R_s$, as shown in Figure 4c where the voltage $V_X(j\omega)$ is assumed at the infinity but actually located at Point X during recording (Figure 4b). When the electrode is present, $Z'_e = Z_e + R_s$ (Figure 4c) is the *conventional electrode impedance* measured in an open-field physiologically relevant electrolyte using electrochemical impedance spectroscopy (EIS), assuming faradaic processes are not involved during the measurement (*i.e.* the faradaic resistance $R_f = \infty$). Thus, $R_s$ appears to belong to the signal source, which generates $V_X(j\omega)$ from $I_X(j\omega)$.

In Figure 4a, an AC amplifier is used, in contrast to the DC amplifier used in conventional intracellular recording under current-clamp mode, where a finite faradic resistance exists in the EDL (Figure 1) [16, 22]. Considering the AC nature of neural signals, since no current flows in the reference electrode path, the negative terminal of the amplifier is shorted to the *GND*, and the full circuit in Figure 4a is equivalent to the one in Figure 4b, which is a current splitter at Point X combined with a voltage divider at Point Y. The voltage $V_{in}(j\omega)$ appearing across the differential amplifier's input terminals at Point Y is related to the field potential $V_X(j\omega)$ at Point X through (3)–(5):

$$V_{in}(j\omega) = \frac{Z'_{ain}}{Z_e + Z'_{ain}} V'_X(j\omega) \tag{3}$$

where $V'_X(\omega)$ is the potential at Point X in the presence of the recording electrode:

$$\begin{aligned} V'_X(j\omega) &= \frac{(Z_e + Z'_{ain})R_s}{Z_e + Z'_{ain} + R_s} I_X(j\omega) = \frac{Z_e + Z'_{ain}}{Z_e + Z'_{ain} + R_s} R_s I_X(j\omega) \\ &= \frac{Z_e + Z'_{ain}}{Z_e + Z'_{ain} + R_s} V_X(j\omega) = \frac{Z_e + Z'_{ain}}{Z'_e + Z'_{ain}} V_X(j\omega) \end{aligned} \tag{4}$$

Substituting (4) into (3), we have,

$$V_{in}(j\omega) = \frac{Z'_{ain}}{Z_e+Z'_{ain}+R_s} V_X(j\omega) \quad (5)$$

Therefore, for extracellular electrical recording using a free-standing point electrode that doesn't form a tight seal with the cell membrane, $R_s$ (*e.g.*, from the outer surface of a 10 μm diameter spherical neuron to *GND* at the infinity, $R_s = \frac{\rho}{4\pi r} = 1{,}433\ \Omega$) is orders of magnitude smaller than the serial impedance $Z_e + Z'_{ain}$ (*e.g.*, >10 MΩ), we thus have

$$V_{in}(j\omega) \approx \frac{Z'_{ain}}{Z_e+Z'_{ain}} V_X(\mathrm{j}\omega) \quad (6)$$

According to (4), the presence of the wired electrode at Point X tends to slightly lower its potential, as $\left|\frac{Z_e+Z'_{ain}}{Z'_e+Z'_{ain}}\right| < 1$. If $R_s \ll |Z_e + Z'_{ain}|$, we have

$$V'_X(j\omega) = \frac{1}{1+\frac{R_s}{Z_e+Z'_{ain}}} V_X(j\omega) \approx V_X(j\omega) \quad (7)$$

Then, this distortion is minute and negligible. It is also noted that the presence of the electrode alone at Point X without providing an additional path to the *GND* (*e.g.*, via the amplifier terminal, thus we can assume $Z'_{ain} = \infty$) doesn't perceivably affect the AC potential at Point X.

Equation (6) proves that the electrode recording system functions as a voltage-divider circuit (attenuating the amplitude) with a first-order highpass filtering effect (narrowing the waveform, formed by $C_{dl}$ (*e.g.* 353 pF for a 30 μm diameter gold planar electrode [22]) and the input resistance $R_{ain}$ (*e.g.* 10 MΩ) of the amplifier with a typical -3 dB cutoff frequency of 45 Hz) to sense the AC potential in an electrolyte where the recording electrode is placed. It is noted that the *electrode recording impedance* $Z_e$ is lumped together with $R_s$ to form the *conventional electrode impedance* $Z'_e$ (Figure 4c), which means conceptually the voltage source is located at the infinity where the *GND* used to be placed, even if the $V_X(j\omega)$ is actually present at Point X, the edge of the electrode's EDL. Nonetheless, in Figure 4c, the voltage drop across $R_s$ is negligible, so that $V'_X(j\omega) \approx V_X(j\omega)$, as shown in (7). However, this sensing mechanism is only made possible by virtue of capacitive current transmission through the EDL of the electrode. This implies that *the voltage $V_{in}(j\omega)$ sensed by the electrode recording system is actually caused by the capacitive current that crosses the electrode's EDL and is in the form of ion redistribution on the electrolyte side*. According to this voltage-divider circuit, when an ionic current flows into the electrode's EDL (*i.e.*, cations flow into or anions flow out of the EDL), a positive voltage is recorded at Point Y; and when an ionic current flows away from the EDL (*i.e.*, cations flow out of or anions flow into the EDL), a negative voltage is recorded.

### *3.3 Basic relationship between extracellular field potential and iAP*

To derive the extracellular field potential $V_X(j\omega)$, we need first to find the net outward transmembrane current $I_E(j\omega)$ during the AP. Assuming an extracellular Point X is located in an isopotential plane through which the $I_E(j\omega)$ flows outward, the potential on this plane is thus determined by $I_E(j\omega)$ and equals to $V_X(j\omega) = R_s I_E(j\omega)$, where $R_s$ is the spreading resistance from this isopotential plane to the *GND* at infinity. Corresponding to the three AP component currents, this isopotential plane sees three ionic currents flowing outward through it: a membrane capacitive current $I_{C0}(j\omega) = I_{Stim}(j\omega)$, $-I_{Na}(j\omega)$ and $I_K(j\omega)$, so that in the subthreshold depolarization phase, $I_{Esub}(j\omega) = I_{Stim}(j\omega)$ and during the AP, $I_{EAP}(j\omega) = -I_{AP}(j\omega)$. According to $V_X(j\omega) = R_s I_E(j\omega)$, $I_{Esub}(j\omega)$ and $I_{EAP}(j\omega)$ produce two sequential extracellular field potential phases in the isopotential plane with

$$V_{Xsub}(j\omega) = R_s I_{Esub}(j\omega) = R_s I_{Stim}(j\omega) \quad (8)$$

$$V_{XAP}(j\omega) = R_s I_{EAP}(j\omega) = -R_s I_{AP}(j\omega) \quad (9)$$

Comparing to (1) and (2), during the subthreshold depolarization phase, we have

$$V_{Xsub}(j\omega) = R_s C_m \cdot j\omega V_{msub}(j\omega) \quad (10)$$

and during the AP, we have

$$V_{XAP}(j\omega) = -R_s C_m \cdot j\omega V_{mAP}(j\omega) \quad (11)$$

From (10) and (11), we see that during the subthreshold depolarization phase, the extracellular field potential $V_{Xsub}(j\omega)$ is proportional to the *first time derivative* of the $V_{msub}(j\omega)$, whereas during the AP, $V_{XAP}(j\omega)$ is proportional to the *negative first time derivative* of the $V_{mAP}(j\omega)$. These relationships result because the same set of AP component currents produce the $V_m(j\omega)$ by charging the membrane capacitor $C_m$, whereas producing the $V_X(j\omega)$ through $R_s$. The amplitude of $V_X(j\omega)$ depends on the overall cell surface area (determines $C_m$) and the distance that the isopotential plane is away from the outer cell surface (determines $R_s$). Note that, according to (10), *any extracellularly recorded subthreshold potentials, e.g. synaptic potentials, are also biphasic in their full cycle*.

A frequent question is why the amplitude of the extracellular field potential $V_X(j\omega)$ is so small comparing to that of the iAP $V_m(j\omega)$. According to (11), this is because the coefficient $R_s C_m \omega$ is very small. An alternative interpretation according to (9) is that (a) the net outward transmembrane current $I_{EAP}(j\omega) = -(I_{Na}(j\omega) - I_K(j\omega))$ is substantially diminished due to mutual cancellation of the opposing $I_{Na}(j\omega)$ and $I_K(j\omega)$, and (b) $R_s$ is small. Moreover, as $I_{EAP}(j\omega)$ propagates into the resistive extracellular space to generate a field potential in the vicinity of the cell according to $V_{XAP}(j\omega) = R_s I_{EAP}(j\omega) = \frac{I_{EAP}(j\omega)}{4\pi\sigma r}$, where $\sigma = \frac{1}{\rho}$ is the

conductivity of the electrolyte and $r$ is the distant Point X is away from the location of the (point) current source [8], the magnitude of $V_{XAP}(j\omega)$ decays with a $1/r$ characteristic. The actual decay with distance from the soma in *in vitro* and *in vivo* settings should be faster than this $1/r$ characteristic of a Coulomb potential around a point source with an infinite current sink [8], due to the presence of adjacent current sinks (*e.g.*, other cells or cellular processes). The edge of this potential field is set by the ionic diffusion limit of $I_{EAP}(j\omega)$ in the electrolyte. At this edge, $I_{EAP}(j\omega)$ attenuates to zero, thus this edge is shorted to the *GND* at the infinity by the intermediate electrolyte solution.

It should be noted that we cannot directly compare the iAP with the extracellular recording by a free-standing point electrode in an open electrolyte, because (a) the two recording systems (Figure 3 and 4) place their *GND*s at different locations, so that the two types of recorded potentials don't have a common reference to compare with, and (b) the two different *GND* placements are incompatible in the same system for simultaneous recordings (*i.e.*, if the *GND* is placed adjacent to the cell, as in a patch-clamp setup, the extracellular recording by the point electrode would be shorted to the *GND* due to the very low resistance of the electrolyte in-between). Fortunately, the transmembrane potential difference is a physical quantity independent from the *GND* placement, so that we can still derive a quantitative relationship between it and the extracellular recording thanks to the shared AP component currents. However, particular to the sealed recording environment of planar substrate electrodes (see below), extracellular and intracellular recordings can be performed in the same setup, thanks to the moderately high electrical resistance $R_{seal}$ (*e.g.*, 0.1~1.2 MΩ [4, 19]) of the cell membrane-electrode seal that separates the recording electrode surface from the exterior bulk electrolyte where the *GND* is placed as part of the intracellular recording setup.

### *3.4 Extracellular recording using a planar substrate microelectrode*

Modeling of the neuron-substrate electrode junctional interfaces has been reported by several groups over the past three decades [5, 22-26]. However, these mere simulation work didn't provide an intuitive analytical solution that offers a clear image on the recording mechanism, nature of the signal, and interplays between key interface parameters. Thus, this is the goal of the current effort.

Figure 5 illustrates the equivalent electrical circuit models based on the aforementioned pioneering work, but with critical new developments (see *Section 3.1* and *3.2*) in pursuit of a closed-form analytical solution. During subthreshold depolarization (Figure 5a), a positive ionic current $I_{Stim}(j\omega)$, either applied artificially or from synaptic inputs, is injected intracellularly to depolarize the membrane. Consequently, the capacitive currents $I_{Cnm}(j\omega)$ and $I_{Cjm}(j\omega)$ with $I_{Cnm}(j\omega) +$

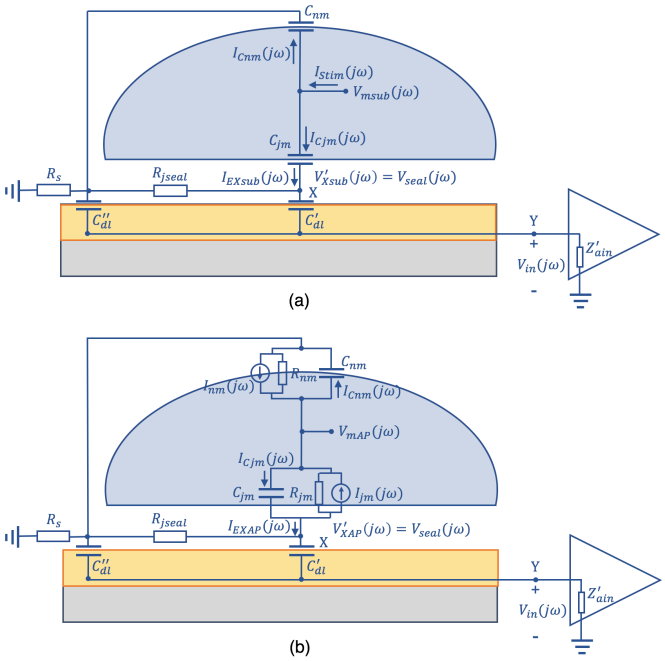


**Figure 5.** Abstracted models of the planar microelectrode-cell membrane interfaces and their equivalent electrical circuits. (a) The equivalent electrical circuit during the subthreshold depolarization phase. (b) The equivalent electrical circuit during the AP.

$I_{Cjm}(j\omega) \approx I_{Stim}(j\omega)$ are transmitted across the membrane to close the circuit. The extracellular current $I_{EXsub}(j\omega)$ responsible for generating the extracellular field potential $V_{Xsub}(j\omega)$ at Point X equals to $I_{Cjm}(j\omega)$. This $I_{Cjm}(j\omega)$ is minimally affected by presence of the membrane-substrate junctional seal (modelled electrically by $R_{jseal}$) [17], so that the entire cell membrane can be considered to have a uniform transmembrane capacitive current density and $I_{Cjm}(j\omega)$ can be approximated as $\beta_{jm}I_{Stim}(j\omega)$, where $\beta_{jm}$ is the percentage of the junctional membrane area to the entire cell membrane area. In absence of the electrode conductor,

$$V_{Xsub}(j\omega) = R_{jseal}I_{jm}(j\omega) + R_s\left(I_{Cjm}(j\omega) + I_{Cnm}(j\omega)\right) = (\beta_{jm}R_{jseal} + R_s)I_{Stim}(j\omega) \quad (12)$$

Comparing to equation (1), we have

$$V_{Xsub}(j\omega) = (\beta_{jm}R_{jseal} + R_s)C_m \cdot j\omega V_{msub}(j\omega) \quad (13)$$

During AP (Figure 5b), the cell membrane acts as an electromotive force (*e.g.*, a battery), and the $I_{Na}(j\omega)$ and $I_K(j\omega)$ result from intrinsic properties of the membrane and don't depend on the presence of $R_{jseal}$, so that the transmembrane current density in the junctional membrane is not affected by the junctional seal. We have $I_{jm}(j\omega) = \beta_{jm}I_{AP}(j\omega)$, where $I_{AP}(j\omega) = I_{jm}(j\omega) + I_{nm}(j\omega)$ is the overall transmembrane AP current. In this case, $I_{EXAP}(j\omega) = -I_{jm}(j\omega)$ (Note that $I_{Cnm}(j\omega)$ and $I_{Cjm}(j\omega)$ are now virtual capacitive currents as defined before), and

$$V_{XAP}(j\omega) = -R_{jseal}I_{jm}(j\omega) - R_s\left(I_{jm}(j\omega) + I_{nm}(j\omega)\right) = -(\beta_{jm}R_{jseal} + R_s)I_{AP}(j\omega) \quad (14)$$

Comparing to (2), we have

$$V_{XAP}(j\omega) = -(\beta_{jm}R_{jseal} + R_s)C_m \cdot j\omega V_{mAP}(j\omega) \quad (15)$$

From (13) and (15), we see that during subthreshold depolarization, the extracellular field potential $V_{Xsub}(j\omega)$ is proportional to the *first time derivative* of the transmembrane voltage $V_{msub}(j\omega)$, while during AP, $V_{XAP}(j\omega)$ is proportional to the *negative first time derivative* of the iAP $V_{mAP}(j\omega)$. The presence of the junctional seal does substantially boost the amplitude of the field potential with an additional term of $\beta_{jm}R_{jseal}$ in the coefficient comparing to (10) and (11). Fitting empirical data to the parameters (see *Appendix*) gives estimations of $v_{Xsub\_peak} = 1.9$ μV and $v_{mAP\_peak} = -33.7$ μV. $v_{mAP\_peak}$ is in the typical amplitude range of reported extracellular field potentials: -10 ~ -500 μV, whereas $v_{Xsub\_peak}$ is below the noise level ($V_{pp}$: 10~40 μV) of typical commercial multielectrode array systems and thus unobservable by this class of electrodes [5, 27]. Because $R_{jseal}$ (*e.g.*, 0.1~1.2 MΩ [4, 19]) is two to three orders of magnitude higher than $R_s$ (~1 kΩ) and $\beta_{jm} \approx 0.3{\sim}0.5$, the amplitude of $v_{mAP}(t)$ is boosted by 30~500 times comparing to the open-field recording in (11).

When the electrode conductor is considered, let's first assume that the cell covers the entire electrode surface (*i.e.*, $C''_{dl} = 0$ in Figure 5), then $Z_e = \frac{1}{j\omega C'_{dl}}$, and

$$V'_X(j\omega) = \frac{Z_e + Z'_{ain}}{Z''_e + Z'_{ain}} V_X(j\omega) \quad (16)$$

$$V_{in}(j\omega) = \frac{Z'_{ain}}{Z''_e + Z'_{ain}} V_X(j\omega) \quad (17)$$

where $Z''_e = Z_e + R_{jseal} + R_s$ is the *in-situ electrode impedance* of the planar substrate microelectrode with the cell overlying on the microelectrode. If the cell fully covers the electrode, $Z_e$ corresponds to the entire $C_{dl}$ and $Z''_e$ can be measured directly; otherwise, $Z_e$ only corresponds to the covered $C'_{dl}$ as depicted in Figure 5 and $Z''_e$ needs to be extracted from the direct measurement due to the shunting effect of the uncovered $C''_{dl}$.

When patch-clamp whole-cell recording is performed in the same setup, *e.g.* for comparison purpose, $R_s$ is grounded in the vicinity of the nonjunctional membrane (*i.e.*, $R_s = 0$), and (16) and (17) become

$$V'_X(j\omega) = \frac{1}{1 + \frac{R_{jseal}}{Z_e + Z'_{ain}}} V_X(j\omega) \quad (18)$$

$$V_{in}(j\omega) = \frac{Z'_{ain}}{Z_e + R_{jseal} + Z'_{ain}} V_X(j\omega) \quad (19)$$

Interestingly, if the cell only partially covers the electrode surface in Figure 5, the exposed electrode surface (modelled electrically by $C''_{dl}$) functions to shunt the effective input impedance of the amplifier, which has two effects: attenuating the magnitude of $Z'_{ain}$ (*i.e.*, reducing the signal-to-noise ratio (SNR) of the recording) and exerting a first-order low-pass filtering effect (formed by $C''_{dl}$ and $R_{ain}$, *e.g.*, a 15 μm diameter neuron sits in the center of a 30 μm diameter electrode, giving a -3dB cutoff frequency of 60 Hz with $R_{ain} = 10$ MΩ). The larger the exposed electrode area, the worse these effects.

## 4. Optimizing the recording quality

When recording in an open-field electrolyte without a tight seal between the electrode and the cell membrane ((10) and (11)), the extracellular field potential is generally unobservable, as it is below the noise level. Therefore, we use the planar microelectrode recording in Figure 5 as an example to lead the following discussions, while the conclusions can be extended to many other cases where a tight seal is formed at the electrode-cell membrane interface, *e.g.*, the gold mushroom-shaped microelectrode (gMμE) [16, 19, 22] and the nanopillar electrodes of a variety of forms [2, 4, 27]. Because, a planar microelectrode cannot record subthreshold potentials (*e.g.*, postsynaptic potentials, see estimation above) from small mammalian neurons, we focus on (15). Substituting (15) into (17), we have the overall frequency response of the linear-time invariant (LTI) system between the voltage source $V_{mAP}(j\omega)$ and the recorded signal $V_{in}(j\omega)$ as

$$H(j\omega) = \frac{V_{in}(j\omega)}{V_{mAP}(j\omega)} = -\frac{Z'_{ain}(\beta_{jm}R_{jseal} + R_s)C_m}{Z''_e + Z'_{ain}} \cdot j\omega \quad (20)$$

This $H(j\omega)$ is a frequency-shaping filter that modulates the magnitude and phase of the frequency spectrum $V_{mAP}(j\omega)$ of the iAP. If the phase angle $\angle H(j\omega)$ still approximates to $-90°$, $V_{in}(j\omega)$ maintains the negative first time derivative relationship to $V_{mAP}(j\omega)$. Anyway, deconvolution should always be performed to recover $V_X(j\omega)$ from $V_{in}(j\omega)$ [2, 28, 29] based on (17), which is the negative first time derivative of the iAP $V_{mAP}(j\omega)$ according to (15). Next, we investigate how the parameters in (20) influence the SNR of the recording through affecting the magnitude $|H(j\omega)|$. Note, $Z'_{ain}$ and $Z''_e$ are also complex functions of $\omega$.

### *4.1 Factors affecting the SNR*

The quality of a neural recording $r(t) = s(t) + N(t)$, where the signal $s(t)$ is deterministic and the background noise $N(t)$ is a stationary stochastic process, is commonly characterized by the SNR defined as the ratio of the power of the signal to the power of the noise: $SNR = \frac{P_S}{P_N} = \frac{\frac{1}{T}\int_0^T s^2(t)dt}{R_N(0)}$, where $T$ is the duration of an observation interval and $R_N(\tau) = \mathcal{E}[N(t)N(t+\tau)]$ is the autocorrelation function of the noise. According to Parseval's relation [30], $\int_0^T s^2(t)dt = \int_{-\infty}^{+\infty}|s(t)|^2dt = \frac{1}{2\pi}\int_{-\infty}^{+\infty}|S(j\omega)|^2d\omega$, where $s(t)$ is assumed 0 outside the interval $T$ and $S(j\omega)$ is its Fourier transform or power spectrum density. In our particular case where $S(j\omega) = V_{in}(j\omega) = H(j\omega)V_{mAP}(j\omega)$,

$$P_s = \frac{1}{2\pi T}\int_{-\infty}^{+\infty}|H(j\omega)|^2|V_{mAP}(j\omega)|^2d\omega \quad (21)$$

Since $V_{mAP}(j\omega)$ is the frequency spectrum of a given voltage source iAP, the magnitude $|H(j\omega)|$ directly affects $P_s$ and thus the SNR of the recording.

In a planar microelectrode array (MEA) recording environment, sources of noises include the intrinsic thermal and shot noises of the recording circuit and electrical noises picked up by the circuits (*e.g.* line and RF noises, which have different frequency ranges than the neural signal and thus can be filtered out from the final recording). The unremovable intrinsic thermal and shot noises are the background noise $N(t)$ left in the final recording and involved in the calculation of the SNR. Thermal noise is generated in electronics according to Ohm's law $P = I^2R$. Thus, the electrical resistances along the electrical current pathway in the recording channel, including the resistance in the electrode material ($R_e$ in Figure 4), need to be minimized. For a planar microelectrode, $R_e$ is very small and thus can be neglected, as did in Figure 5.

Next, let's scrutinize influences of the parameters and variables in (20) on the $|H(j\omega)|$:

*4.1.1 Constant parameters.* Effects of the constant parameters $C_m$, $\beta_{jm}$, $R_s$, and $R_{jseal}$ to the extracellular field potential $V_{XAP}(j\omega)$ is shown by (15), and consequently, $|H(j\omega)| \propto (\beta_{jm}R_{jseal} + R_s)C_m$. $R_sC_m$ corresponds to contribution from the overall cell membrane capacitive current through the open-field solution spreading resistance $R_s$. According to (11), $R_s$ is insufficient to produce an observable signal above the noise level for small mammalian neurons with a small $C_m$. However, this is not the case for large neurons from the invertebrate such as leech [31] and Aplysia [16, 19, 22]. So, larger cells with a larger $C_m$ helps to improve the SNR. However, the major contribution of $C_m$ is taking effect through $\beta_{jm}C_mR_{jseal}$, the junctional membrane that forms a tight seal with the substrate; and as such, the larger the junctional membrane $\beta_{jm}C_m$, which determines the junctional current $I_{jm}(j\omega)$ in Figure 5b, and the tighter of the membrane-substrate seal, which determines $R_{jseal}$, the higher the SNR [19]. Accordingly, major efforts have been devoted to increase the $R_{jseal}$ and the junctional current for improved recording quality [2, 4, 16, 19, 22, 27, 31-33].

*4.1.2 $Z_e''$ and $Z_{ain}'$.* If the electrode recording system is properly engineered and configured, $C_{lsh} = 0$, $C_{esh} = 0$, and $R_{sc} = \infty$ in Figure 4. Equation (17) describes how the electrode recording system affects the recording of the extracellular field potential $V_{XAP}(j\omega)$. Basically, $Z_e''$ and $Z_{ain}'$ forms a voltage-divider circuit with a frequency response of $\frac{Z_{ain}'}{Z_e''+Z_{ain}'}$. This transmission process both attenuates the signal amplitude and shifts the phase in the effect of a high-pass filter as discussed earlier. This is the reason for the common call for decreasing the electrode's conventional impedance $Z_e'$ via increasing the $C_{dl}$, and increasing the amplifier's input impedance $Z_{ain}$ [7, 34, 35]. However, it needs to be emphasized that it is the electrode recording impedance $Z_e$ corresponding to the cell-covered $C_{dl}'$ (Figure 5) that needs to be decreased (thus $C_{dl}'$ needs to be increased), whereas the uncovered $C_{dl}''$ needs to be decreased. Merely increasing the overall $C_{dl}$ won't necessarily improve the SNR, rather, in cases that the uncovered $C_{dl}''$ is large, can severely diminish the SNR. Therefore, planar electrodes with diameter comparable to that of the overlying cell body are preferred. Under this condition, the larger the $C_{dl}'$, the smaller the amplitude attenuation and the smaller the cutoff frequency of the highpass filter formed by $C_{dl}'$ and $R_{ain}$.

*4.1.3 $R_{jseal}$.* In (20), $R_{jseal}$ appears in both the numerator and denominator. To determine how $|H(j\omega)|$ depends on $R_{jseal}$, we calculate $\frac{\partial|H(j\omega)|}{\partial R_{jseal}}$ and find that it is positive for all $\omega$ and that the larger $|Z_{ain}'|$, the larger its value. This means that (a) a high $R_{jseal}$ can effectively boost the SNR and (b) a high $|Z_{ain}'|$ can further augment this effect. $R_s$ has a similar effect, but as it is usually unchangeable in a recording environment and it is more than two orders of magnitude smaller, its effect is minimum.

### *4.2 Electrode impedance*

As discussed above, the electrode recording impedance $Z_e$ (conventionally measured as $Z_e'$ in an open-field physiologically relevant electrolyte), a part of the *in-situ* electrode impedance $Z_e''$, is one of critical variables influencing the recording SNR and thus a must-have data for any paper that reports either the development of a new type of neural electrode or the neural recording and/or stimulation using an electrode. However, this piece of critical information is frequently either missing or not reported properly in the literature. For example, many papers only reported the magnitude *vs.* frequency plot of the electrode impedance, whereas the phase plot was missing. As the electrode impedance is a complex function of frequency, this make it impossible for the community to (a) develop full knowledge on characteristics of the electrode and (b) use deconvolution to recover $V_X(j\omega)$ from $V_{in}(j\omega)$ as in (17). To make things worse, many studies didn't measure the electrode impedance in a proper manner, resulting in inaccurate or misleading data reported. Thus, I'd like to elaborate and clarify the essential aspects on electrode impedance and its measurement.

*4.2.1 Principle of electrode impedance measurement.* To measure its impedance, the electrode is treated as a an LTI system with a current input $I_e(j\omega)$ and a voltage output $V_e(j\omega)$. Thus, the frequency response $H_e(j\omega) = \frac{V_e(j\omega)}{I_e(j\omega)}$ of the system is the $Z_e'$. For this LTI system, a complex exponential signal $e^{j\omega_1 t}$ with a unique characteristic frequency of $\omega_1$ generates an output as a modulated version of the same

complex exponential [30]: $e^{j\omega_1 t} \xrightarrow{H_e(j\omega)} H_e(j\omega_1)e^{j\omega_1 t} = |H_e(j\omega_1)|e^{j[\omega_1 t+\angle H_e(j\omega_1)]}$, where $|H_e(j\omega)|$ is an even function of $\omega$ and $\angle H_e(j\omega_1)$ is an odd function (therefore, the plots only show the first quadrant). So, the strategy to measure $H_e(j\omega)$ is to construct a sequence $[\omega_1, \omega_2, \omega_3, \cdots, \omega_n]$ in the working frequency range (*e.g.*, 0.01 Hz ~ 100 kHz) of the electrode and measure the corresponding $H_e(j\omega_n)$'s one by one to reconstruct the full profile of $H_e(j\omega)$. In practice, we use a function generator to produce a current signal $Acos\omega_n t$ as the testing input signal and use a frequency spectrum analyzer to analyze the corresponding output voltage signal. According to Euler's relation, the input current $Acos\omega_n t = \frac{A}{2}e^{j\omega_n t} + \frac{A}{2}e^{-j\omega_n t}$, and thus the output voltage of the electrode system is $\frac{A}{2}H_e(j\omega_n)e^{j\omega_n t} + \frac{A}{2}H_e(-j\omega_n)e^{-j\omega_n t} = A|H_e(j\omega_n)|\cos[\omega_n t + \angle H_e(j\omega_n)]$ (see *Appendix* for proof). Therefore, extracting the gain $|H_e(j\omega_n)|$ and phase shift $\angle H_e(j\omega_n)$ from the output will reconstruct the $H_e(j\omega_n) = |H_e(j\omega_n)|e^{j\angle H_e(j\omega_n)}$ at each $\omega_n$. $H_e(j\omega_n)$ is conventionally presented as the magnitude and phase plots in logarithmic scales (see Figure 6 for an example [36]).

*4.2.2 Method for electrode impedance measurement.* The measurement is usually performed using a potentiostat in a three-electrode electrochemical cell comprising a working, a counter, and a reference electrode in PBS. The electrode being measured is connected to the working electrode. There are two options for the counter electrode: A. using an electrode of exactly the same characteristics, *i.e.* materials composition and geometry, or B. using a very large electrode whose impedance can be ignored. The working and counter electrodes need to be placed far apart. As the circuit path being measured includes the working electrode, the PBS, the counter electrode, and the connecting leads (usually neglectable), the measurement $M = Z_{we} + R_s + Z_{ce} + R_{leads}$. In case A, $Z'_e = \frac{M}{2} = Z_{we} + \frac{R_s+R_{leads}}{2} \approx Z_e + R_s$; and in case B, $Z'_e = Z_e + R_s \approx M$. Selection for the amplitude $A$ in $Acos\omega_n t$ needs to be as small as possible, *e.g.* 2.5 mV, to avoid potential initiation of faradaic reactions in the EDL of either electrode. Selection for $[\omega_1, \omega_2, \omega_3, \cdots, \omega_n]$ is usually evenly spaced in the logarithmic frequency range.

It should be noted that the testing signal for measuring recording electrode is different from that for stimulation electrode. In the EDL model (Figure 1) of passive recording electrodes, $R_f = \infty$ [2] and the testing signal should not generate any faradaic currents across the EDL. In contrast, almost all stimulation electrodes function under the faradaic regime where $R_f$ is finite; and thus their measurement should reflect and emulate such a working condition (beyond the scope of this current work).

*4.2.3 How to read the impedance plots.* While the role of $|Z'_e|$ in affecting the recording SNR is generally well understood (see above and (5)), the frequent missing of the phase plot in literature reflects a lack of knowledge on the meaning of this piece of data [37]. Referring first to Figure 6a—the magnitude *vs.* frequency plot in log-log scales, the impedance magnitude of the Pt electrode has the well-recognizable shape: starting with a very high value at a frequency (*e.g.* 0.1 Hz) close to DC, the curve declines linearly (exponentially in a linear scale) due to the decease of $\frac{1}{j\omega C_{dl}}$ with frequency until a transiting region and then becomes a flat line at high frequencies where the frequency is large enough to make $\frac{1}{j\omega C_{dl}} \approx 0$. The earlier the curve declines to the transiting point (indicated by the arrow in Figure 6a), the larger the $C_{dl}$, as desired. The value of the flat line is actually the total resistance $R_{total}$ in the measurement circuit, including $R_s$, $R_e$, $R_{leads}$, and contact resistances at joints or

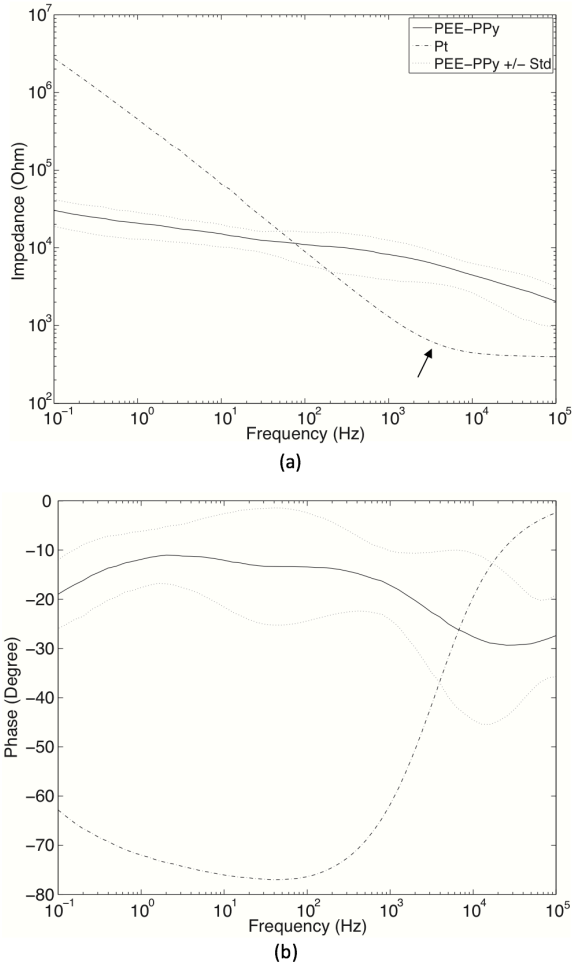


**Figure 6.** Example magnitude (a) and phase (b) plots for the electrode impedance of a recording neural electrode array [34]. The electrodes (1 mm diameter) and leads were directly made of the conducting polymer polypyrrole (PEE-PPy, conductivity: 116.3 ± 7.8 S/cm). Average electrical impedance spectrum with standard deviation of four electrodes are shown. A smooth Pt disc electrode of the same geometric surface area was used as a control. The measurement configuration followed Option B (see main texts) and was the same for both electrode types. Figure reproduced with permission from [36]. Copyright © 2013 WILEY-VCH Verlag GmbH & Co. KGaA, Weinheim.

connections if any. For this particular Pt electrode, $R_s \approx R_{total} = 400\,\Omega$. With this information, $C_{dl}$ can then be determined from any data point in the lower frequency range. Turning to the phase *vs.* frequency plot in Figure 6b, at low frequencies the phase angle is close to $-90°$, as $\frac{1}{j\omega C_{dl}}$ dominates; and at high frequencies, the curve approaches to $0°$ as $\frac{1}{j\omega C_{dl}}$ zeros out and $Z'_e$ becomes resistive.

By contrast, the impedance of the "active" polypyrrole electrode is more complicated to interpret. The magnitude declines monotonically in the measuring frequency range without flattening at high frequencies, and the phase angle with values around $-20°$ across the frequency range shows a dominant resistive nature. This is because the polypyrrole electrode worked primarily in reversible faradaic processes (thus the word "active" is used) generating a pseudo capacitance to transmit charges across the frequency range even with the 5 mV test sinusoidal signals [38]. Thus, there was a major current path through $R_f$ in the EDL model in Figure 1, and the current path through $C_{dl}$ was only a minor one, making the decay of the magnitude with frequency in Figure 6a much slower. Furthermore, the magnitude is substantially lower at low frequencies, because the electrode surface is porous and much rougher, resulting in a much larger $C_{dl}$. It remains relatively high at high frequencies, because both the lead and electrode were directly made of the semiconducting polypyrrole, thus bearing higher resistances.

Lastly, as the characteristic frequencies of the iAP center around 1 kHz (*i.e.*, the base width of the iAP of a typical neuron is 1 ms), the electrode impedance is frequently measured only at 1 kHz. Although this single point of data is sufficient to calculating the $C_{dl}$ and $R_s$ in the EDL model of a passive neural recording electrode, the aforementioned intuitive information that can be captured from the spectrum plots is unfortunately missing.

*4.2.4 Methods to reduce electrode impedance.* Because passive neural recording electrodes function as a pure capacitor. To reduce the electrode impedance, we need to increase the EDL capacitance (Figure 1) according to $C_{dl} = \varepsilon_0 \frac{Area}{d}$, where $\varepsilon_0$ is permittivity of free space, $Area$ is the equivalent electrochemical surface area of the EDL, and $d$ is the thicknesses of the EDL. As thickness of the Stern layer and the Debye length cannot be changed in physiologically relevant electrolyte, the only option is to increase $Area$ by either roughening the smooth electrode surface [39] or coating it with rough and/or porous conductive materials including platinum black [35], conducting polymers [40, 41] and carbon nanotubes [42].

## 5. Summary

Through a revisit to the essential aspects concerning extracellular neural recording, this paper has developed in-depth new insights on this important electrophysiological technique. Key points and recommendations are summarized below:

- The electrode-electrolyte interface of passive neural recording electrodes functions as a pure capacitor $C_{dl}$, and the extracellular field potential that an electrode senses is at the outer edge of this $C_{dl}$, *i.e.* the outer edge of its EDL.
- The voltage $V_{in}(j\omega)$ recorded by the electrode recording system is caused by the capacitive current that crosses the electrode's EDL and is in the form of ion redistribution on the electrolyte side. When an ionic current flows into the electrode's EDL (*i.e.*, cations flow into or anions flow out of the EDL), a positive voltage is recorded; and when an ionic current flows away from the EDL (*i.e.*, cations flow out of or anions flow into the EDL), a negative voltage is recorded.
- The presence of a wired electrode at a point tends to slightly lower its field potential, however, when disconnected from the amplifier's input terminal, it doesn't perceivably affect the AC field potential at that point.
- The electrode recording system functions as a voltage-divider circuit (attenuating the amplitude) with a first-order highpass filtering effect (narrowing the waveform, formed by $C_{dl}$ and the input resistance $R_{ain}$ of the amplifier) to sense the AC potential in an electrolyte where the recording electrode is placed.
- The extracellular field potential has two phases, with its subthreshold depolarization phase proportional to the first time derivative of the membrane depolarization and its action potential phase proportional to the *negative* first time derivative of the iAP. In particular, any extracellularly recorded subthreshold potentials, e.g. synaptic potentials, are *biphasic* in their full cycle.
- The presence of a junctional seal between the electrode surface and cell membrane greatly enhances the amplitude of the field potential in the junction. However, planar substrate microelectrodes are still incapable of extracellularly detecting subthreshold potentials from small mammalian neurons.
- If the cell only partially covers the electrode surface, the exposed electrode surface ($C''_{dl}$ in Figure 5) functions to shunt the effective input impedance of the amplifier, which has two effects: attenuating the magnitude of $Z'_{ain}$ (*i.e.*, reducing the SNR of the recording) and exerting a first-order low-pass filtering effect (formed by $C''_{dl}$ and $R_{ain}$). The larger the exposed electrode area, the worse these effects.
- The recorded voltage $V_{in}(j\omega)$ is related to the extracellular field potential $V_X(j\omega)$ by (5) or (17). This is the reason for the common call for decreasing the electrode's conventional impedance $Z'_e$ via increasing the $C_{dl}$, and increasing the amplifier's input impedance $Z_{ain}$. However, it needs to be emphasized that it is the electrode recording

impedance $Z_e$ corresponding to the cell-covered $C'_{dl}$ (Figure 5) that needs to be decreased (thus $C'_{dl}$ needs to be increased), whereas the uncovered $C''_{dl}$ needs to be decreased. Merely increasing the overall $C_{dl}$ won't necessarily improve the SNR, rather, in cases that the uncovered $C''_{dl}$ is large, can severely diminish the SNR. Therefore, planar electrodes with diameter comparable to that of the overlying cell body are preferred. The selection of $Z_{ain}$ is advised to be at least one order of magnitude higher than $Z'_e$.

- The electrode impedance, conventionally measured as $Z'_e$ in an open-field physiologically relevant electrolyte, must be reported for any paper that reports either the development of a new type of neural electrode or the neural recording using an electrode. The report should include both the magnitude and phase plots. The measurement should be performed with a proper setup (e.g., Option A or B), and the testing signal should not generate any faradaic currents across the EDL.

## Appendix

### *Parameters Used for Calculations of $v_{Xsub\_peak}$ and $v_{mAP\_peak}$ in Section 3.4*

Rat cortical neuron [2]: $r = 7.5$ μm, $C_{jm} = 1.77$ pF, $C_{nm} = 3.53$ pF, $C_m = 5.3$ pF, $R_{jseal} = 0.1$ MΩ, rising phase: $\frac{\Delta V_m}{\Delta t} = \frac{90\ mV}{0.5\ ms} = 180\ V/s$, $\frac{\Delta V_{msub}}{\Delta t} = \frac{10\ mV}{1\ ms} = 10\ V/s$.

$$v_{Xsub\_peak} = \left(\frac{1}{3} \times 0.1\ M\Omega + 2\ \text{k}\Omega\right) \times 5.3\ pF \times 10\frac{V}{s} = 1.9\ \mu\text{V}$$

$$v_{XAP\_peak} = -\left(\frac{1}{3} \times 0.1\ M\Omega + 2\ \text{k}\Omega\right) \times 5.3\ pF \times 180\frac{V}{s} = -33.7\ \mu\text{V}$$

### *Proof for the Principle of Electrode Impedance Measurement*

$$\begin{aligned}
&\frac{A}{2}H_e(j\omega_n)e^{j\omega_n t} + \frac{A}{2}H_e(-j\omega_n)e^{-j\omega_n t} \\
&\quad = \frac{A}{2}\left[H_e(j\omega_n)e^{j\omega_n t} + H_e^*(j\omega_n)e^{-j\omega_n t}\right] \\
&\quad = \frac{A}{2}\cdot 2\mathcal{R}e\{H_e(j\omega_n)e^{j\omega_n t}\} \\
&\quad = A\mathcal{R}e\left\{|H_e(j\omega_n)|e^{j[\omega_n t + \angle H_e(j\omega_n)]}\right\} \\
&\quad = A|H_e(j\omega_n)|\cos[\omega_n t + \angle H_e(j\omega_n)]
\end{aligned}$$

## Acknowledgements

This work was supported in part by the U.S. National Science Foundation under Grant Number 1749701 and the U.S. Defense Advanced Research Projects Agency under Grant Number D17AP00031. The views, opinions, and/or findings contained in this article are those of the author and should not be interpreted as representing the official views or policies, either expressed or implied, of the Defense Advanced Research Projects Agency or the Department of Defense.

## References

[1] C. Gold, D. A. Henze, C. Koch, and G. Buzsaki, "On the origin of the extracellular action potential waveform: A modeling study," *J Neurophysiol,* vol. 95, no. 5, pp. 3113-28, May 2006.

[2] J. T. Robinson, M. Jorgolli, A. K. Shalek, M. H. Yoon, R. S. Gertner, and H. Park, "Vertical nanowire electrode arrays as a scalable platform for intracellular interfacing to neuronal circuits," *Nat Nanotechnol,* vol. 7, no. 3, pp. 180-4, Jan 10 2012.

[3] A. Hai and M. E. Spira, "On-chip electroporation, membrane repair dynamics and transient in-cell recordings by arrays of gold mushroom-shaped microelectrodes," *Lab on a Chip,* vol. 12, no. 16, pp. 2865-2873, 2012.

[4] M. Dipalo *et al.*, "Intracellular and Extracellular Recording of Spontaneous Action Potentials in Mammalian Neurons and Cardiac Cells with 3D Plasmonic Nanoelectrodes," (in English), *Nano Letters,* vol. 17, no. 6, pp. 3932-3939, Jun 2017.

[5] M. E. Spira and A. Hai, "Multi-electrode array technologies for neuroscience and cardiology," *Nature nanotechnology,* vol. 8, no. 2, pp. 83-94, 2013.

[6] P. Massobrio, G. Massobrio, and S. Martinoia, "Interfacing Cultured Neurons to Microtransducers Arrays: A Review of the Neuro-Electronic Junction Models," (in English), *Frontiers in Neuroscience,* vol. 10, Jun 21 2016.

[7] M. J. Nelson, P. Pouget, E. A. Nilsen, C. D. Patten, and J. D. Schall, "Review of signal distortion through metal microelectrode recording circuits and filters," (in English), *Journal of Neuroscience Methods,* vol. 169, no. 1, pp. 141-157, Mar 30 2008.

[8] K. W. Horch and G. S. Dhillon, *Neuroprosthetics: theory and practice*. World Scientific, 2004.

[9] J. Huang, Z. Li, H. Ge, and J. B. Zhang, "Analytical Solution to the Impedance of Electrode/Electrolyte Interface in Lithium-Ion Batteries," (in English), *Journal of the Electrochemical Society,* vol. 162, no. 13, pp. A7037-A7048, 2015.

[10] I. Valov, "Interfacial interactions and their impact on redox-based resistive switching memories (ReRAMs)," (in English), *Semiconductor Science and Technology,* vol. 32, no. 9, Sep 2017.

[11] D. K. Kampouris, X. B. Ji, E. P. Randviir, and C. E. Banks, "A new approach for the improved interpretation of capacitance measurements for materials utilised in energy storage," (in English), *Rsc Advances,* vol. 5, no. 17, pp. 12782-12791, 2015.

[12] L. Pilon, H. N. Wang, and A. d'Entremont, "Recent Advances in Continuum Modeling of Interfacial and Transport Phenomena in Electric Double Layer Capacitors," (in English), *Journal of the Electrochemical Society,* vol. 162, no. 5, pp. A5158-A5178, 2015.

[13] C. V. Chaparro, L. V. Herrera, A. M. Meléndez, and D. A. Miranda, "Considerations on electrical impedance measurements of electrolyte solutions in a four-electrode cell," *Journal of Physics,* no. Conference Series 687, p. 012101, 2016.

[14] P. Fromherz, "Electrical interfacing of nerve cells and semiconductor chips," *Chemphyschem,* vol. 3, no. 3, pp. 276-84, Mar 12 2002.

[15] S. F. Cogan, "Neural stimulation and recording electrodes," (in English), *Annual Review of Biomedical Engineering,* vol. 10, pp. 275-309, 2008.

[16] A. Hai, J. Shappir, and M. E. Spira, "In-cell recordings by extracellular microelectrodes," (in English), *Nature Methods,* vol. 7, no. 3, pp. 200-U50, Mar 2010.

[17] L. Guo, "On neural recording using nanoprotrusion electrodes," *Journal of neural engineering,* 2019.

[18] D. Johnston and S. M.-s. Wu, *Foundations of cellular neurophysiology*. Cambridge, Mass.: MIT Press, 1995, pp. xxxi, 676 p.

[19] A. Hai *et al.*, "Spine-shaped gold protrusions improve the adherence and electrical coupling of neurons with the surface of micro-electronic devices," (in English), *Journal of the Royal Society Interface,* vol. 6, no. 41, pp. 1153-1165, Dec 6 2009.

[20] J. J. FitzGerald, S. P. Lacour, S. B. McMahon, and J. W. Fawcett, "Microchannel electrodes for recording and stimulation: in vitro evaluation," *IEEE Trans Biomed Eng,* vol. 56, no. 5, pp. 1524-34, May 2009.

[21] J. J. Fitzgerald, S. P. Lacour, S. B. McMahon, and J. W. Fawcett, "Microchannels as axonal amplifiers," *IEEE Trans Biomed Eng,* vol. 55, no. 3, pp. 1136-46, Mar 2008.

[22] A. Hai, J. Shappir, and M. E. Spira, "Long-Term, Multisite, Parallel, In-Cell Recording and Stimulation by an Array of Extracellular Microelectrodes," (in English), *Journal of Neurophysiology,* vol. 104, no. 1, pp. 559-568, Jul 2010.

[23] A. Hierlemann, U. Frey, S. Hafizovic, and F. Heer, "Growing Cells Atop Microelectronic Chips: Interfacing Electrogenic Cells In Vitro With CMOS-Based Microelectrode Arrays," (in English), *Proceedings of the Ieee,* vol. 99, no. 2, pp. 252-284, Feb 2011.

[24] P. Fromherz, "Electrical interfacing of nerve cells and semiconductor chips," (in English), *Chemphyschem,* vol. 3, no. 3, pp. 276-284, Mar 12 2002.

[25] M. Grattarola and S. Martinoia, "Modeling the neuron-microtransducer junction: from extracellular to patch recording," *IEEE Trans Biomed Eng,* vol. 40, no. 1, pp. 35-41, Jan 1993.

[26] M. Jenkner and P. Fromherz, "Bistability of membrane conductance in cell adhesion observed in a neuron transistor," (in English), *Physical Review Letters,* vol. 79, no. 23, pp. 4705-4708, Dec 8 1997.

[27] C. Xie, Z. L. Lin, L. Hanson, Y. Cui, and B. X. Cui, "Intracellular recording of action potentials by nanopillar electroporation," (in English), *Nature Nanotechnology,* vol. 7, no. 3, pp. 185-190, Mar 2012.

[28] C. Rossant, B. Fontaine, A. K. Magnusson, and R. Brette, "A calibration-free electrode compensation method," (in English), *Journal of Neurophysiology,* vol. 108, no. 9, pp. 2629-2639, Nov 2012.

[29] C. Rossert, H. Straka, S. Glasauer, and L. E. Moore, "Frequency-domain analysis of intrinsic neuronal properties using high-resistant electrodes," (in English), *Frontiers in Neuroscience,* vol. 3, 2009.

[30] A. V. Oppenheim and A. S. Willsky, *Signals and Systems*, 2nd Edition ed. Prentice Hall, 1997.

[31] M. Jenkner and P. Fromherz, "Bistability of membrane conductance in cell adhesion observed in a neuron transistor," *Physical review letters,* vol. 79, no. 23, p. 4705, 1997.

[32] Z. L. C. Lin, C. Xie, Y. Osakada, Y. Cui, and B. X. Cui, "Iridium oxide nanotube electrodes for sensitive and prolonged intracellular measurement of action potentials," (in English), *Nature Communications,* vol. 5, Feb 2014.

[33] A. Cohen, J. Shappir, S. Yitzchaik, and M. E. Spira, "Reversible transition of extracellular field potential recordings to intracellular recordings of action potentials generated by neurons grown on transistors," (in English), *Biosensors & Bioelectronics,* vol. 23, no. 6, pp. 811-819, Jan 18 2008.

[34] E. Castagnola *et al.*, "Smaller, softer, lower-impedance electrodes for human neuroprosthesis: a pragmatic approach," *Frontiers in neuroengineering,* vol. 7, p. 8, 2014.

[35] S. Arcot Desai, J. D. Rolston, L. Guo, and S. M. Potter, "Improving impedance of implantable microwire multi-electrode arrays by ultrasonic electroplating of durable platinum black," *Frontiers in neuroengineering,* vol. 3, p. 5, 2010.

[36] L. Guo, M. Ma, N. Zhang, R. Langer, and D. G. Anderson, "Stretchable polymeric multielectrode array for conformal neural interfacing," *Adv Mater,* vol. 26, no. 9, pp. 1427-33, Mar 2014.

[37] A. V. Oppenheim and J. S. Lim, "The Importance of Phase in Signals," (in English), *Proceedings of the Ieee,* vol. 69, no. 5, pp. 529-541, 1981.

[38] L. Guo, "Conducting Polymers as Smart Materials for Tissue Engineering," in *Fundamental Principles of Smart Materials for Tissue Engineering* Q. Wang, Ed. no. RSC Smart Materials Series): Royal Society of Chemistry, 2017.

[39] X. Y. Cui and D. C. Martin, "Fuzzy gold electrodes for lowering impedance and improving adhesion with electrodeposited conducting polymer films," (in English), *Sensors and Actuators a-Physical,* vol. 103, no. 3, pp. 384-394, Feb 15 2003.

[40] X. Y. Cui and D. C. Martin, "Electrochemical deposition and characterization of poly(3,4-ethylenedioxythiophene) on neural microelectrode arrays," (in English), *Sensors and Actuators B-Chemical,* vol. 89, no. 1-2, pp. 92-102, Mar 1 2003.

[41] M. R. Abidian and D. C. Martin, "Multifunctional nanobiomaterials for neural interfaces," *Advanced Functional Materials,* vol. 19, no. 4, pp. 573-585, 2009.

[42] E. W. Keefer, B. R. Botterman, M. I. Romero, A. F. Rossi, and G. W. Gross, "Carbon nanotube coating improves neuronal recordings," (in English), *Nature Nanotechnology,* vol. 3, no. 7, pp. 434-439, Jul 2008.